Transport of polymer particles in oil-water flow in porous media: enhancing oil recovery

M.A. Endo Kokubun · F.A. Radu · E. Keilegavlen · K. Kumar · K. Spildo

Abstract We study a heuristic, core-scale model for the transport of polymer particles in a two phase (oil and water) porous medium. We are motivated by recent experimental observations which report increased oil recovery when polymers are injected after the initial waterflood. We propose the recovery mechanism to be microscopic diversion of the flow, where injected particles can accumulate in narrow pore throats and clog it, in a process known as a log-jamming effect. The blockage of the narrow pore channels lead to a microscopic diversion of the water flow, causing a redistribution of the local pressure, which again can lead to the mobilization of trapped oil, enhancing its recovery. Our objective herein is to develop a core-scale model that is consistent with the observed production profiles. We show that previously obtained experimental results can be qualitatively explained by a simple two-phase flow model with an additional transport equation

M.A. Endo Kokubun
Department of Chemistry, University of Bergen, Allégaten 41, 5007 Bergen, Hordaland, Norway
Tel.: +47 55 58 34 44
E-mail: max.kokubun@uib.no

F.A. Radu
Department of Mathematics, University of Bergen, Allégaten 41, 5007 Bergen, Hordaland, Norway
E-mail: florin.radu@uib.no

E. Keilegavlen
Department of Mathematics, University of Bergen, Allégaten 41, 5007 Bergen, Hordaland, Norway
E-mail: eirik.keilegavlen@uib.no

K. Kumar
Department of Mathematics, University of Bergen, Allégaten 41, 5007 Bergen, Hordaland, Norway
E-mail: kundan.kumar@uib.no

K. Spildo
Department of Chemistry, University of Bergen, Allégaten 41, 5007 Bergen, Hordaland, Norway
E-mail: kristine.spildo@uib.no

for the polymer particles. A key aspect of the formulation is that the microscopic heterogeneity of the rock and a dynamic altering of the permeability must be taken into account in the rate equations.

1 Introduction

After initial waterflood, a large quantity of oil is still left inside the reservoir, with remaining oil ratios frequently exceeding 50% of the total amount (Lake et al, 1992). Techniques to recover this remaining oil are known as tertiary recovery methods (enhanced oil recovery) and many different approaches have been proposed (Sheng, 2011) (in-situ combustion, steam injection, polymer injection, microbial enhanced recovery, etc). The choice of one or another recovery method depends on a myriad of factors, ranging from economical costs, geological characteristics of the reservoir, thermophysical properties of the remaining oil, geographical location of the reservoir, etc.

Table 1 Nomenclature

Nomenclature	
A_1, A_2	constants for residual oil saturation change
c_l	mass concentration of polymer particles (kg/m^3)
$\mathbf{D_l}$	Diffusion matrix of polymer particles in water (m^2/s)
d_p	polymer particle diameter (m)
$\mathbf{g}$	gravity vector (m/s^2)
$\mathbf{K}$	absolute permeability tensor (m^2)
K_B	Boltzmann constant (m^{2}kg/s^{2}K)
k_l	constant rate of clogging (m^{-1})
k_r	constant rate of unclogging (s^{-1})
$k_{r\alpha}$	relative permeability of phase α
n_o, n_w	exponents for the relative permeabilities
p_α	pressure of phase α (Pa)
R	reaction rate (kg/m^{3}s)
s_α	saturation of phase α
T	temperature (K)
$\mathbf{u}_\alpha$	velocity of phase α (m/s)
Greek letters	
γ	constant for permeability change
δ	heterogeneity factor
λ_α	mobility of phase α (m s/kg)
μ_α	viscosity of phase α (kg/m s)
ρ_α	mass density of phase α (kg/m^3)
σ	volumetric concentration of accumulated particles
τ	tortuosity
ϕ	porosity
φ	clogging rate (kg/m^{3}s)
ψ	unclogging rate (kg/m^{3}s)

Injecting nanoparticles along with water into the reservoir have the potential to enhance oil recovery. There are several different types of nanoparticles that can be used in such process of enhancement of oil recovery, but most of the studies focus on nanoparticles that can change the wettability of the rock, thus changing capillary pressure curves and improving oil recovery (El-Amin et al, 2013). In the case of nanoparticles that interact with the rock (through electrostatic potential, for example (Bennacer et al, 2017; Ray et al, 2012)), attachment rates must be considered in order to account for the deposition of the particles at pore walls. (Borazjani et al, 2017)

Colloidal dispersion gels (CDG) refers to systems consisting of low concentration of polymer and crosslinker, typically partially hydrolyzed polyacrylamide and aluminium citrate. At these low concentrations, a solution of separate gel bundles (Mack and Smith, 1994) or polymer particles (Spildo et al, 2009, 2010) forms. CDG have been successfully used for enhancing oil recovery in field while lowering water production (Mack and Smith, 1994; Chang et al, 2006). The mechanism behind the increased recovery is, however, still not clear.

Diversion of injection fluids from high-permeability into low-permeability zones (Chang et al, 2006; You et al, 2013; Abdulbaki et al, 2014), improved mobility ratio (Shi et al, 2011) and microscopic flow diversion (Spildo et al, 2009, 2010) are some of the proposed driving mechanisms. In the latter case, the polymer particles are assumed to accumulate in pore throats when the particle-carrying water flows from a large to a narrow pore. Accumulation occurs due to inertia effects: when the water flow from the large to the narrow pore throat, it accelerates. Due to inertia, particles tend to be left behind, such that incoming particles can catch up and accumulate at the pore entrance. This may lead to diversion of the flow into neighbouring, oil-containing pores, and thus increased recovery. The proposed mechanism was supported by core flooding data which demonstrated that the effect of increased water viscosity on recovery was not sufficient to explain the observed increase in oil recovery, and that recovery was higher for cores with more heterogeneous pore size distributions (Spildo et al, 2009). In this paper we will explore the hypothesis that microscopic diversion is the responsible for the enhancement of oil recovery. Moreover, in this work we refer to CDG as polymer particles.

The injected polymer particles can accumulate in narrow pore throats, leading to a log-jamming effect that essentially diverts the water flow. A schematic is shown in Fig. 1. When a pore throat is clogged, the water is diverted towards the oil-containing neighbouring pore channel. If the pressure increase in the oil-containing channel is large enough, the remaining oil is mobilized and can be recovered. After oil is mobilized, conditions may favour unclogging of the pore throat (see section 2.1). Since the characteristics of the polymer particles are such that they do not change the wettability of the rock, microscopic diversion of the flow is one of the main responsible for enhancing oil recovery during polymer particle injection.

Polymer particles are complex particles which are formed by mixing a low concentration aqueous-polymer solution with a crosslinker. Effects that can contribute to oil mobilization include viscosity changes of the polymer-carrying water, absorption, incomplete complexation of polymers and crosslinkers, which can lead to polymer- and particle-carrying with different flow properties, and log-jamming. If the complexation between crosslinkers and polymer is incomplete, some pure polymer might be injected along with the polymer particles. If that is

the case, the governing equations should distinguish between two polymer-carrying and particles-carrying water, as these have different effects on flow properties (in addition to a conservation equation for the oil phase). Nevertheless, pore network models have shown that log-jamming plays a more prominent role in permeability reduction and variation in the core pressure difference, when compared to viscosity change, polymer straining and adsorption (Bolandtaba et al, 2009; Bolandtaba and Skauge, 2011). Therefore, as a first approach one can construct a simple model which neglects incomplete complexation, straining and adsorption in the governing equations, thus neglecting polymer-carrying water effects. This first approach can then be used as a starting point for constructing more realistic models, which take into account the complex physical interactions of this problem.
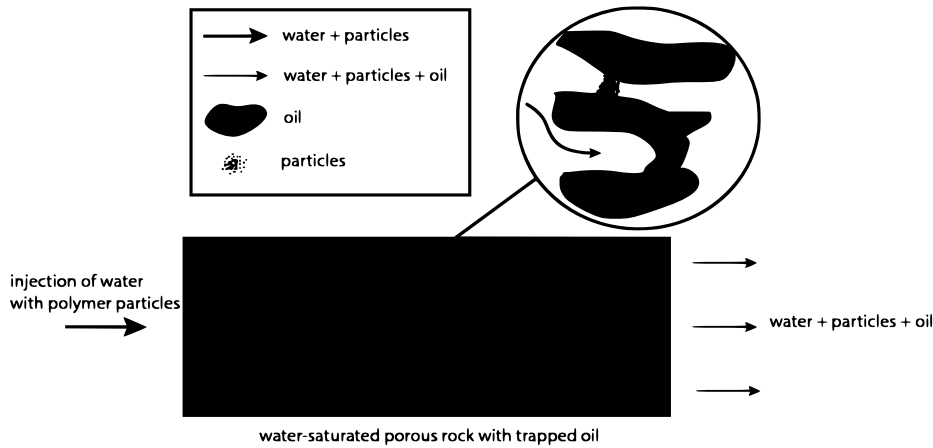

Fig. 1 Polymer particles injected along with water flow into a porous rock with trapped oil. The clogging of a pore channel and the consequent water flow diversion leading to the recovery of initially trapped oil is shown in the detail.

Some recent experimental results (Spildo et al, 2009, 2010) have shown that injection of polymer particles along with water into a rock containing trapped oil exhibit some different characteristics when compared to other particle-carrying systems (such as fines migration or nanoparticle injection). For example, even though the enhancement in oil recovery is prominent, measurements of pressure drops along the core have shown that some of the tested cores exhibited a very small final permeability reduction. This indicates that unclogging occurred after oil mobilization took place. Moreover, measurements in Berea sandstone cores showed negligible enhancement in oil recovery due to polymer particle injection, which suggests that some cores may be more suitable to polymer particle injection as an enhanced oil recovery method than others. It is our intention, in this paper, to develop a simple mathematical model that correctly mimics the experimental results described in (Spildo et al, 2009, 2010), by identifying what we believe to be the relevant physical mechanisms present in this problem.

Due to the local nature of the relevant processes that influence the log-jamming effect (pressure difference in each pore, different particle concentrations and veloc-

ities, etc), and the intrinsic nature of upscaled models (which consider averaged values for the quantities of interest in a representative volume that contains a statistically significant amount of pores), no rigorous modelling of particle accumulation in two-phase flow in porous media are available. Therefore, we study a simple heuristic, core-scale model that takes into account the transport of polymer particles diluted in the water phase and the mechanisms of clogging and unclogging of pores. We consider a non-equilibrium reaction for the accumulation and release of particles at the narrow pore throats. A key aspect that must be taken into account is that the heterogeneity of the rock, specifically in the pore throat radius distribution, has a significant role on the particle accumulation process (Spildo et al, 2009). This can be explained by pore-scale acceleration and inertia effects for particle-carrying water, which will be more pronounced in heterogeneous rocks (de Anna et al, 2017). Our model accounts for this effect by relating the reaction coefficient in the model for accumulation to the distribution of pore throat sizes. We further include reductions in the residual oil saturation due to the presence of particles.

This papers is structured as follows. In section 2 we present the model, introducing the rate equation, with an emphasis on the conceptual model of log-jamming. In section 3 we present some numerical solutions to the model. First we present a representative case in order to highlight the main characteristics of the model and then we compare our results with the available experimental data. We finalize the paper with the Conclusions. In the Appendix we present the heterogeneity parameter for the cores utilized in previous experiments (Spildo et al, 2009).

2 Model formulation

We consider that polymer particles are transported only by the water phase and do not interact with the oil phase, i.e., mass transfer between phases and possible interface effects are neglected. The water and oil phase mass conservation equations are given by

$$\frac{\partial}{\partial t}\left(\phi s_\alpha\right) + \nabla \cdot \mathbf{u}_\alpha = 0, \tag{1}$$

where $\alpha \in \{w, o\}$, denotes the water and oil phase, respectively, ϕ is the porosity, s_α the saturation of phase α and $\mathbf{u}_\alpha$ is the Darcy velocity of phase α. The flow is considered incompressible, which means that variations in pressure are not considered high. The velocity of phase α is given by Darcy's law

$$\mathbf{u}_\alpha = -\boldsymbol{K}\lambda_\alpha\left(\nabla p_\alpha - \rho_\alpha\mathbf{g}\right), \tag{2}$$

where $\lambda_\alpha = k_{r\alpha}/\mu_\alpha$ is the mobility of phase α, with viscosity μ_α and relative permeability $k_{r\alpha}$. The relative permeability depends on the saturation of phase α, while the absolute permeability tensor $\boldsymbol{K}$ depends on the rock properties.

The size of the injected particles vary in a narrow range around 100 nm. However, when experimentally preparing the polymer particles, the aqueous solution is filtered prior to injection (Spildo et al, 2010). Therefore, we assume that there is only a single size for the injected particles. The polymer particles are transported by the water phase and can accumulate in narrow pore throats. Denoting by c_l the

mass concentration of polymer particles, the advection-diffusion transport equation is given by

$$\frac{\partial}{\partial t} \left(\phi s_w c_l + \rho_l \sigma \right) + \nabla \cdot \left(\mathbf{u}_w c_l - \boldsymbol{D}_l \phi s_w \nabla c_l \right) = 0, \tag{3}$$

where σ is the volumetric concentration of polymer particles that have been trapped due to log-jamming and ρ_l is the mass density of the polymer particles. We consider Fick's law for diffusion of mass, with $\boldsymbol{D}_l$ as the diffusion matrix of polymer particles.

The volumetric concentration of accumulated particles σ is obtained from the following rate equation

$$\rho_l \frac{\partial \sigma}{\partial t} = R, \tag{4}$$

where R is a non-equilibrium rate function that takes into account accumulation and release of particles in narrow pore throats. The general nonlinear form of R is given by

$$R = \varphi(\phi, c_l, \sigma, u_w) - \psi(\phi, c_l, \sigma), \tag{5}$$

where φ and ψ are the accumulation and removal functions of the particles, respectively and $u_w = |\boldsymbol{u}_w|$ is the magnitude of the water velocity. The proper form of the reaction rate will be discussed in the next section.

2.1 Log-jamming and particle release

As far as the authors are aware, no rigorously derived expression for R exists in the literature. One of the major difficulties associated with its derivation is the fact that log-jamming is a process which intrinsically depends on pore-scale physics. Therefore, a comprehensive model would have to be derived from the analysis of the conservation equations at the pore-scale, and then upscaled in order to obtain the reaction rate as a function coupled to the pore-scale physics (Bringedal et al, 2016; Bringedal and Kumar, 2017; Muntean and Nikolopoulos, 2017). To derive a rigorous upscaled model for two-phase flow, including the transport of particles, is outside the scope of this work. Instead, we chose a heuristic construction for the reaction rate based on the a priori knowledge of the main physical aspects of the problem.

When the particles clog a pore, water flow is diverted, and the diverted water may mobilize initially-trapped oil located in neighbouring pores. After clogging a pore, the accumulated particles may eventually be remobilized, unclogging the pore and restoring the water flow in it. The clogging particles are brought to the pore by advection of water, such that we consider that the accumulation of particles is proportional to the convective flux of the particles $u_w c_l$. We consider that when a pore channel is clogged, the flow is completely diverted to neighbouring channels, such that there is no accumulation of particles behind the clog. This implies that there is no filtration of water through the accumulated particles.

Experimental results indicate that cores with a higher degree of microscopic heterogeneity tend to have a higher accumulation of particles, which leads to higher recovery rates (Spildo et al, 2009). This can be explained by the fact that when water flows from a large to a narrow pore throat, it accelerates. Polymer particles

are heavier than water, rendering them with a delayed response time with respect to changes in the surrounding flow field. Consequently, the particles accumulate at the pore entrance due to inertia effects, which may lead to clogging of the channel if enough accumulate. Particles usually have a diameter smaller than the pore throat diameter, such that a single particle can not block a pore. In the proposed mechanism for log-jamming, the large-to-small pore throat radius ratio is more relevant, as it induces to abrupt changes in the flow field, which enhances inertia effects. We quantify this change by introducing a macroscopic measure of the microscopic rock heterogeneity into the rate of log-jamming.

Consider the two pore size distributions shown in Fig. 2(a). The bimodal distribution, shown as a solid line, represents a heterogeneous core (taken from (Spildo et al, 2009)), with two predominant pore throat radii. The unimodal distribution, shown as a dashed line, represents a homogeneous core used for comparison (Berea). Their cumulative distribution functions are shown in Fig. 2(b). We consider the Kolmogorov-Smirnov statistics (Stephens, 1974), which is a measure of the maximum separation between the two cumulative distribution curves, as an indicator of the degree of microscopic heterogeneity. Denoting the maximum separation as $\delta \in [0, 1]$, we can see that $\delta = 0$ represents a homogeneous rock, whereas $\delta = 1$ represents a highly heterogeneous rock. Since log-jamming occurs when particle-carrying water flows from the large pores to the narrow pores, δ measures the strength of log-jamming in the core. A more detailed explanation of the δ parameter is given in the Appendix.
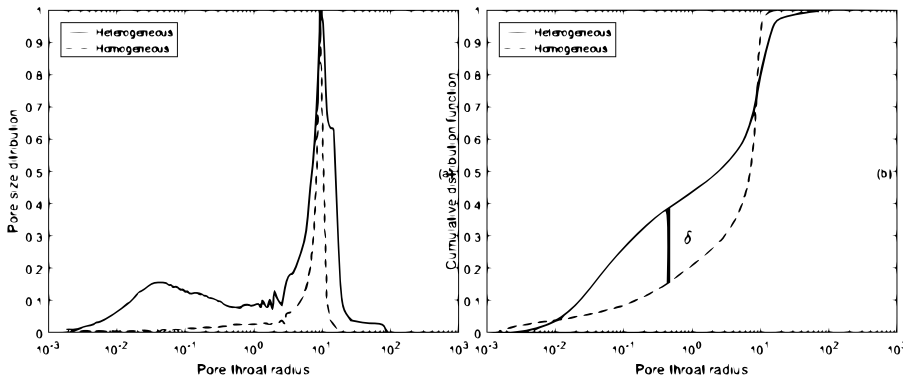

Fig. 2 (a) Pore-throat distributions for a heterogeneous and a homogeneous core; and (b) their respective cumulative distribution functions.

The unclogging of pore throats is a complex phenomenon to model. For the transport of fine particles, as the ones released during low salinity waterflood, for example, an increase in the pressure above a certain critical value is enough to force particles through the constriction (or break them) (Civan, 2016). However, such effect requires that filtration of water between the accumulated particles takes place. Since after a pore throat is clogged the water flow is diverted to a neighbouring channel, no significant filtration of water through the particles is expected. We consider that unclogging occurs as a result of the pressure release from the water flow behind the accumulated particles when the water flow is completely diverted.

This is analogous to considering a relaxation time for the accumulation of particles. After the pressure behind the clog is relieved due to complete diversion of the water flow, the particles move by diffusion in the static water, restoring possible water paths through them. Eventually, filtration of water can be restored and the particles advected through the unclogged pore. A schematic is shown in Fig. 3. According to this proposed mechanism, unclogging is mostly dependent on the volumetric concentration of accumulated particles. For simplicity, we consider this dependence to be linear.
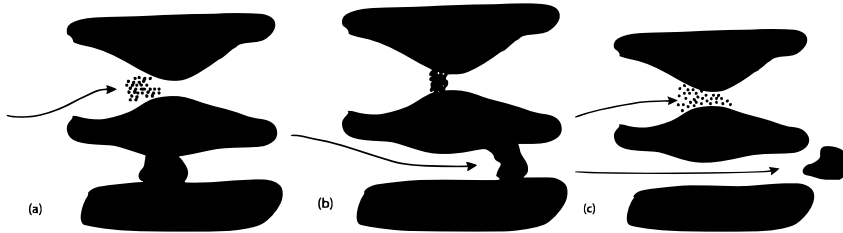

Fig. 3 (a) Water flowing into the upper channel, leading to the accumulation of particles and clogging of the pore. (b) Water flow is completely diverted towards to the lower channel, mobilizing the trapped oil. (c) The pressure release behind the accumulated particles leads to the restoration of the water filtration in the upper channel, eventually leading to unclogging of the pore.

Note that our conceptual model considers that there are no interaction between the particles and the rock wall. This is justified by the fact that polymer particles are negatively charged (Bjørsvik et al, 2008), such that attractive interactions between polymer particles and negatively charged sandstones, such as Berea (Nasralla and Nasr-El-Din, 2014), are unlikely to occur. Therefore, we consider that clogging of the pore is purely a mechanical effect. We point here that if charged ions are transported along with the polymer particles, interactions between them and the negatively-charged rock may occur. Nevertheless, we neglect such possibility and focus instead on the transport of stable polymer particles, in order to analyse the effect of log-jamming.

For simplicity, at this stage we choose simple relations for the accumulation and removal functions, $\varphi(\phi, c_l, \sigma, u_w) = \varphi(\phi, c_l, u_w)$ and $\psi(\phi, c_l, \sigma) = \psi(\sigma)$, respectively in Eq. (5). Therefore, we consider the following rate equation

$$R = \delta(\phi k_l u_w c_l - k_r \rho_l \sigma) \qquad (6)$$

where k_l and k_r are constant rates accounting for clogging and unclogging and δ is the proportionality constant. One can see from Eq. (6) that in a complete homogeneous medium, i.e., when $\delta = 0$, log-jamming does not occur. Equation (6) is a modified version of the rate equation presented by Gruesbeck and Collins (Gruesbeck and Collins, 1982), where they studied particle accumulation in a single-phase flow in a porous medium and neglected the detachment rate. Moreover, the rock heterogeneity was not taken into account in their work. Therefore, in comparison to the rate equation presented in (Gruesbeck and Collins, 1982), we consider the effects of porosity ϕ, water velocity u_w, heterogeneity δ and unclogging rate $-k_r \rho_l \sigma$.

It is worth to mention that not only the pore-size distribution is relevant for log-jamming, but also how the pores are connected. For example, it is possible that many of the narrow pore throats are not connected to the larger pores, such that log-jamming is not favoured. In fact, the connectivity of the pores is a key factor for determining the occurrence of log-jamming. The hydrodynamic properties of the particles in the pore channel are also relevant with regards to determining whether unclog will occur or not. Without a detailed knowledge of the water pathways inside the core, one can not expect to construct a complete model at this moment.

In the present model we neglect deposition and removal of particles at pore walls. Log-jamming completely blocks a water pathway, whereas particle deposition lowers the area available for the water flux in the pore proportionally to the particle surface area, but it does not divert the water flow. Therefore, the permeability reduction caused by log-jamming is expected to be more severe than the one caused by deposition. We do account for a local lowering of porosity by particle accumulation, by the model

$$\phi = \phi_0 - \sigma, \tag{7}$$

where ϕ_0 is the initial porosity.

Sequential clogging of pore channels will lead to the microscopic diversion of the water flow into neighbouring pore channels. This may lead to the displacement of initially trapped-oil, i.e., an increase in the amount of oil available for mobilization. In the next section we discuss this effect.

2.2 Residual oil saturation

After waterflood, the remaining oil is divided between capillary-trapped oil and oil which is trapped in some channels where water does not flow (as schematically shown in Fig. 1). For capillary-trapped oils, the forces acting at the water-oil interface are weaker than the attachment force of oil at the pore wall, preventing its mobilization. The remaining oil, on the other hand, is oil located in pore channels where water does not flow, thus preventing its mobilization. Capillary-trapped oil may be mobilized through an increase in the capillary number (a ratio between viscous force and interfacial tension between water and oil) (Sheng, 2011), while the remaining trapped oil may be mobilized through a microscopic diversion of the water flow from the narrow channels into the larger pore channels containing trapped oil.

These two processes are fundamentally distinct, such that different strategies need to be used for each apart. Techniques such as injection of surfactants (Sheng, 2011) and microbial enhanced oil recovery (Landa-Marbán et al, 2017), aim at increasing the capillary number and recover capillary-trapped oil. Injection of polymer particles, on the other hand, aims at recovering trapped oil through clogging of the narrow water paths, leading to a microscopic diversion of the water flow into larger channels where oil is initially trapped. One must note that microscopic diversion of the flow occurs at the pore-scale, which makes it distinct to diversion of flow to low-permeability areas (a core-scale process).

While these two processes are different from on the pore scale, on the core scale they are both manifested as an increase in the amount of oil available for mobilization. This can be reproduced through a lowering on the residual oil saturation on the model. In the literature there is an abundance of models for the residual oil saturation based on the capillary number, but none regarding the microscopic diversion of water flow, as far as the authors are aware. For simplicity, we adapt a model taken from Li *et al* (Li et al, 2007), hence considering the residual saturation as a function of the accumulated particles as

$$s_{or} = \min\left(s_{or}, s_{or}^{min} + (s_{or}^{ini} - s_{or}^{min})[1 + (A_1\sigma)^{A_2}]^{1/A_2-1}\right), \tag{8}$$

where A_1 and A_2 are constants which determine the rate at which residual oil saturation lowers, s_{or}^{min} is the absolute minimum value for the residual oil saturation and s_{or}^{ini} is the initial residual oil saturation. In the context of the present discussion, s_{or}^{min} may be seen as the non-recovered capillary-trapped oil.

2.3 Parametrizations

The changes in porosity given by (7) induce changes in permeability. There are many models in the literature relating permeability and porosity (Jacquin, 1964; Adler et al, 1990). Ultimately, this relation depends on the detailed pore structure of the rock. The accumulation of particles will lead to a linear decay in the porosity according to (7). We utilize the following relation for the permeability (Hussain et al, 2013)

$$\frac{K}{K_0} = \frac{1}{1 + \gamma(\phi_0 - \phi)} = \frac{1}{1 + \gamma\sigma}, \tag{9}$$

where γ is a constant.

The phase mobilities $\lambda_\alpha = k_{r\alpha}/\mu_\alpha$ depends on the saturation s_α through the relative permeabilities $k_{r\alpha}(s_\alpha)$. The viscosities are constant, as we assume that the flow is isothermal. We consider a power-law of the Corey-Brooks type (Brooks and Corey, 1964) for the relative permeabilities

$$k_{ro} = (1 - s_w^*)^{n_o}, \quad k_{rw} = (s_w^*)^{n_w}, \tag{10}$$

where n_o and n_w are constants, and s_w^*

$$s_w^* = \frac{s_w - s_{wi}}{1 - s_{or} - s_{wi}} \tag{11}$$

is the effective water saturation, with s_{or} and s_{wi} the residual oil saturation and irreducible water saturation, respectively. The irreducible water saturation s_{wi} does not change during injection of polymer particles, while the residual oil saturation s_{or} changes according to Eq. (8).

For the capillary pressure, we consider

$$p_c = -p_e \ln(s_w^*), \tag{12}$$

where p_e is an entry pressure. Note that Eq. (12) does not account for hysteresis or dynamical effects (van Duijn et al, 2016). In essence, we consider an equilibrium model for the capillary pressure.

If we consider the polymer particles as spheres with an average diameter of d_p, the diffusion coefficient may be calculated using the Stokes-Einstein relation

$$D = \frac{\tau K_B T}{2\pi \mu_w d_p},$$

(13)

where K_B is the Boltzmann constant, T is the absolute temperature and τ is the constant that measures the tortuosity of the flow. Even though dispersion is usually larger than diffusion in porous media, we neglect it for simplicity. Our main goal is to analyse the effect of particle accumulation and flow diversion. Moreover, even though we consider very small values for D, it is necessary to keep the diffusion coefficient for numerical reasons.

The set of Eqs. (1)–(4) models the transport of polymer particles in the water phase in a oil-water flow, considering the log-jamming rate as given by (6). By providing proper initial and boundary conditions, the problem can be solved numerically.

3 Numerical results

The model presented in the previous section was implemented in MRST (Matlab Reservoir Simulation Toolbox) (Lie, 2016), an open-source reservoir simulator, which contains a vast range of data structures and computational methods implemented. For our problem, we consider the EOR (Enhanced Oil Recovery) module and implement our model based on the polymer model presented there (Bao et al, 2017).

The spatial domain is discretized in a simple 3D cartesian grid with one block in both y and z directions, such that, essentially, a 1D model is considered. The fluxes are calculated on the cell faces, whereas the variables are cell-centered quantities. Therefore, the model equations are discretized using a first-order implicit scheme in time and a standard two-point spatial scheme with upstream weighting, assuring mass conservation at each grid cell. The discrete equations are then cast into residual form and a Newton method is employed to obtain the numerical solutions. The standard tolerance for the Newton solver embedded in MRST is of 10^{-8}.

3.1 Model capabilities

Before we compare the results obtained from the present model with the experimental data given in (Spildo et al, 2009), we present some illustrative numerical results in order to highlight the main properties of the model. For such, we neglect gravity and capillary effects and consider a domain of length $L = 2\ m$, area $4 \times 10^{-2}\ m^2$, initial permeability $K_0 = 1\ \mu m^2$ and initial porosity $\phi_0 = 0.3$. The diffusion coefficient D is calculated for coreflooding occurring at $T = 358.15\ K$ (Spildo et al, 2009), water viscosity $\mu_w = 0.29\ mPa \cdot s$, polymer particles of diameter $d_P = 40\ \mu m$ and tortuosity $\tau = 5$. We have the following parameters (the values of the reaction rates were chosen from dimensional analysis)

The remaining parameters are given by $A_1 = 10, A_2 = 1 \times 10^4$ and $\gamma = 2 \times 10^3$. The backpressure is kept fixed at $p(L,t) = 10^5\ Pa$, whereas the injection rate of

Table 2 Parameters used for numerical calcuations.

$D = 3 \times 10^{-11} \ m^2/s$	$\mu_o = 3.6 \ mPa \cdot s$
$k_l = 10^3 \ m^{-1}$	$\rho_l = 1100 \ kg/m^3$
$k_r = 10^{-6} \ s^{-1}$	$\delta = 1$
$s_{or}^{ini} = 0.5$	$n_w = 2.5$
$s_{wi} = 0.05$	$n_o = 3.0$

water is kept at $1.67 \times 10^{-6} \ m^3/s$ at $x = 0$. Initial and boundary conditions are given respectively by

$$t = 0: \quad s_w(x,0) = 0.06, \quad c_l(x,0) = 0. \tag{14}$$

$$x = 0, t > 0: \quad s_w(0,t) = 1, \quad c_l(0,t) = 1 \ (kg/m^3) \ H(t-t_l)(1-H(t-t_w)). \tag{15}$$

We start injecting particles at a mass concentration of $1 \ kg/m^3$ at $t = t_l$, the time at which oil production due to injection of pure water ceases. When $t = t_w$, we stop injecting polymer particles and perform a postwater flush for $t > t_w$. The time t_w is when oil production due to polymer particle injection decrease. Therefore, the water viscosity (in $mPa \cdot s$) is given by (Spildo et al, 2009)

$$\mu_w = \begin{cases} 0.29, & t < t_l \text{ and } t > t_w, \\ 0.90, & t_l < t < t_w, \end{cases} \tag{16}$$

In Fig. 4(a), we show the profiles of c_l and σ for the beginning of the particle front propagation. The polymer particles start to propagate downstream (from left to right) a smooth front, connecting the initial value $c_l = 0$ to some value $c_l < c_l^{inj}$, which is smaller than the injection value because of the particle accumulation in the upstream side of the front. Then, the oil saturation profile connects $c_l < c_l^{inj}$ to c_l^{inj} at the injection point $x = 0$. At the time step shown in Fig. 4(a), the accumulation of particles is low, such that the flow is essentially non-disturbed. This can be seen in Fig. 4(b), where the profiles for oil and water saturation are shown for the same time step.
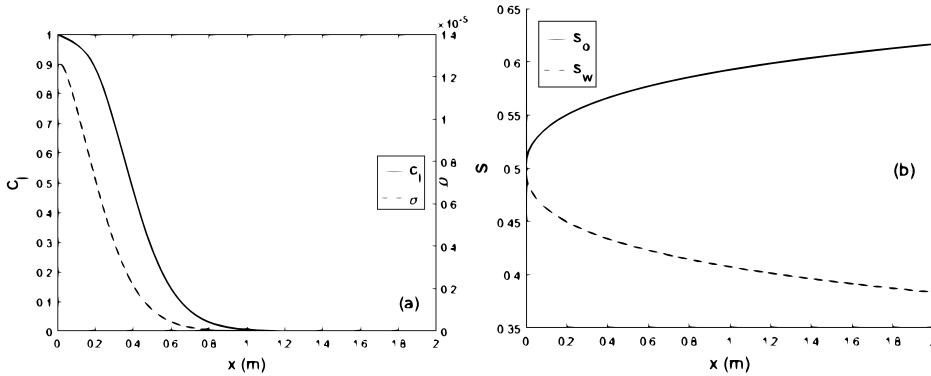

Fig. 4 (a) Mass concentrations of polymer and volumetric concentration of accumulated particles. (b) Oil and water saturation. Flow direction is from left to right.

   The accumulation of particles in the upstream side of the particle front eventually is large enough to clog some pore channels, leading to the mobilization of initially trapped oil through a lowering on the residual oil saturation according to Eq. (8). The newly mobile oil is displaced by the water flow upstream, which creates non-monotone oil saturation and particle concentration profiles. The oil front eventually evolves into two shock fronts. The slower shock, which is preceded by a rarefaction wave, is located at the point where the residual oil saturation change from s_{or}^{min} to s_{or}^{ini}. The faster shock is a typical Buckley-Leverett oil-water shock, but jumping from a high oil saturation to a low oil saturation downstream. These features can be seen in Figs. 5(a) and (b). For the last time snap shown in Fig. 5(b), the slower shock is located between $x = 1$ and $x = 1.6$, approximately, and it is diffuse because the transition from s_{or}^{min} to s_{or}^{ini} is smooth. For this same time snap in the same figure, the faster shock is located around $x = 1.8$. The dual shock structure shown in Fig. 5(b) is similar to the one present in surfactant injection, and therefore their velocities can be calculated using standard Buckley-Leverett theory (Pope, 1980).
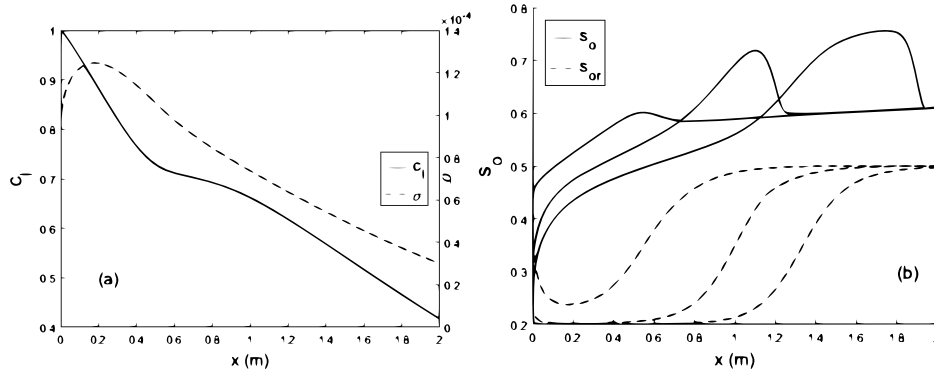

Fig. 5 (a) Mass concentrations of polymer and volumetric concentration of accumulated particles when trapped oil begins to be mobilized. (b) Oil saturation at different time steps, showing the formation of a dual-shock structure.

   When the oil front reaches the outlet, recovery increases significantly. In Fig. 6(a) we present the oil recovery (in percentage of original oil initially in place) and the pressure drop across the core. We inject pure water for a period of 10 pore volumes, after which we begin to inject water with polymer particles for a period of 25 pore volumes, before postwashing it with pure water for 5 pore volumes. Accumulation of particles behind the particle front leads to displacement of initially trapped oil. The final amount of oil recovered is determined by the strength of the reaction rate and by the minimum residual oil saturation s_{or}^{min}. According to our assumptions, s_{or}^{min} corresponds to the oil that remains capillary-trapped after mobilization of trapped oil through log-jamming and it can not be recovered through particle accumulation. The lowering in the residual oil saturation in this case was of 52%.

   The pressure drop along the core increases as production of oil takes place, decreasing to a steady value when only the injected phase is produced at the outlet.

There is a new decrease in the pressure drop when we cease injection of polymer particles and replace it by injection of pure water (postwater flush) due to viscosity decrease. As injected particles begin to clog pore channels, permeability reduction takes place and the pressure drop increases in comparison with pure waterflood. The pressure drop along the core is inversely proportional to the permeability K and the total mobility $\lambda = \lambda_w + \lambda_o$. If we neglect capillary pressure and gravity, the ratio between the pressure drops after postwater flush ΔP_{pw} and waterflood ΔP_{wf} is given by

$$\frac{\Delta P_{pw}}{\Delta P_{wf}} = \left(\frac{K^0}{K^F} \right) \left(\frac{\lambda^0}{\lambda^F} \right), \tag{17}$$

where the superscripts 0 and F denote initial and final values, respectively. Accumulation of particles leads to a decline in the core permeability, while lowering in the residual oil saturation leads to an increase in the mobility. Thus, these two processes have opposite effects in the overall pressure drop. In the present case, we have a pressure drop ratio of 2.00, a permeability reduction of 62% and a mobility ratio of 1.32. During the postwater flush, only unclogging occurs, as particles are no longer injected into the core. This causes the slight decrease in the pressure drop between 35 and 40 pore volumes, as seen in Fig. 6(a).

In Fig. 6(b) we show the particle effluent as a ratio of the concentration of particles at the outlet and the injected particles. The particle front travels ahead of the oil front, carried by the water flow. Under the conditions given in Table 2, the particle front reaches the outlet prior to the oil front (first increase shown in Fig. 6(b), right after 10 pore volumes). When oil starts to be produced at the outlet (at around 11 pore volumes), the effluent of particles decrease abruptly because of the lower water content, increasing again as oil production ceases. After production of oil ceases, the effluent of particles is mainly determined by the competition between clogging and unclogging. An equilibrium state is achieved when $R = 0$, i.e., when clogging and unclogging balance each other according to Eq. (6). From Fig. 6(a), one can see that for times after around 17 pore volume injected, the pressure drop across the core begins to lower. This is an effect of unclogging becoming more relevant than clogging, i.e., $R < 0$. In this case, one can see from Fig. 6(b) that between 25 and 35 of pore volumes injected, the particle effluent is complete.

3.2 Comparison with experimental results

In this section we compare numerical results with the experimental data taken from (Spildo et al, 2009). The experiments described in (Spildo et al, 2009) were conducted in five different cores, from which we take three for comparison[1], with different rock properties. After the initial preparation of the cores, the experiments had three stages: waterflood at a rate of 1.67×10^{-9} m/s, waterflood at a rate of 1.67×10^{-8} m/s, injection of polymer particles with water at a rate of 1.67×10^{-8} m/s and a post water flush at the same rate (water with no particles). We fix some parameters and vary the available rock properties in order to compare

---

[1] For the other two cores: one was not stabilized during polymer particle injection and the other achieved pressure drops one order of magnitude higher than the other cores, such that we considered those two cores to be outside the parametric range for comparison considered here.
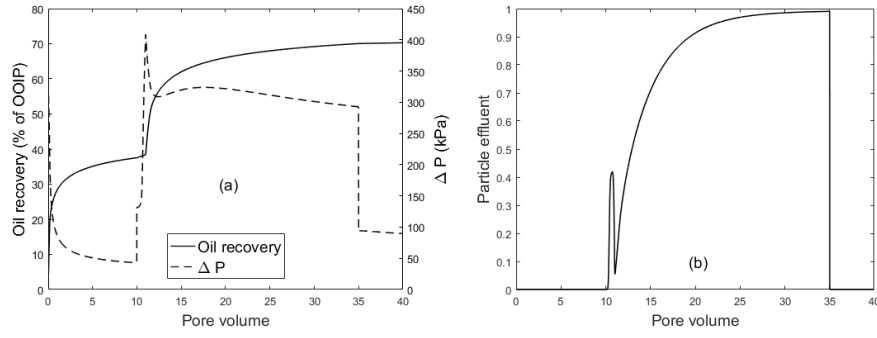
Fig. 6 (a) Oil recovery and pressure drop. (b) Particle effluent normalized with respect to the injected concentration. The sudden decrease in the particle effluent around 11 pore volumes occurs when the oil front reaches the outlet.

our results with the reported experimental results. The varying parameters will be the initial rock permeability K_0, initial porosity ϕ_0, initial residual oil saturation s_{or}^{ini}, irreducible water saturation s_{wi} and rock heterogeneity δ, all of which are taken from (Spildo et al, 2009). The unclogging constant k_r is then fitted to match the final permeability reduction. The rock heterogeneity is calculated as explained in section 2.1 using the available data for the pore-size distribution of each representative core (see Appendix A). The unclogging constant is varied in order to adjust the final pressure drop ratio.

The cores have similar sizes and for simplicity we consider the same length of $L = 0.2\ m$ and cross-sectional area $9 \times 10^{-4}\ m^2$ for the three cores. The specific values for each core are given in Table 3. The entry pressure p_e, necessary for the capillary pressure, is given by $p_e = 10^3\ Pa$, whereas the clogging constant is given by $k_l = 2 \times 10^4\ m^{-1}$. It is worth to mention that the backpressure $p(L,t)$ and the entry pressure p_e are one order of magnitude smaller than the real values considered in the experiments (Spildo et al, 2009). This is due to numerical restrictions: we are considering a small domain, such that high values for the pressure would cause variations too large to be handled by the numerical solver. Otherwise specifically stated, the remaining parameters are the same as the ones given in Table 2.

Table 3 Data varied from core to core.

	Core A	Core B	Core C
$K_0(\mu m^2)$	0.90	0.50	0.30
ϕ_0	0.33	0.32	0.33
s_{or}^{ini}	0.51	0.30	0.32
s_{or}^{min}	0.20	0.17	0.19
s_{wi}	0.06	0.18	0.24
δ	0.2315	0.0540	0.0354
$k_r(s^{-1})$	2.0×10^{-8}	1.2×10^{-4}	4.0×10^{-4}

Initial and boundary conditions are given respectively by

$$t = 0: \quad s_w(x,0) = s_{wi} + 0.01, \quad c_l(x,0) = 0. \tag{18}$$

$$x = 0, t > 0: \quad s_w(0,t) = 1.0, \quad c_l(0,t) = 1 \ (kg/m^3) \ H(t - t_l)(1 - H(t - t_w)). \tag{19}$$

The initial condition is such that the core is mostly oil-saturated prior to water-flood. Injection of polymer particles along with water only occurs after some time t_l, which is chosen as the time when oil production ceases after the second water-flood. When oil production ceases during the stage of particles injection (which occurs at a time t_w), we start injecting pure water (post water flush). As mentioned previously, we consider two stages of waterflood before the injection of polymer particles. The rates considered as boundary conditions are the same as the ones utilized in the experiments conducted in (Spildo et al, 2009).
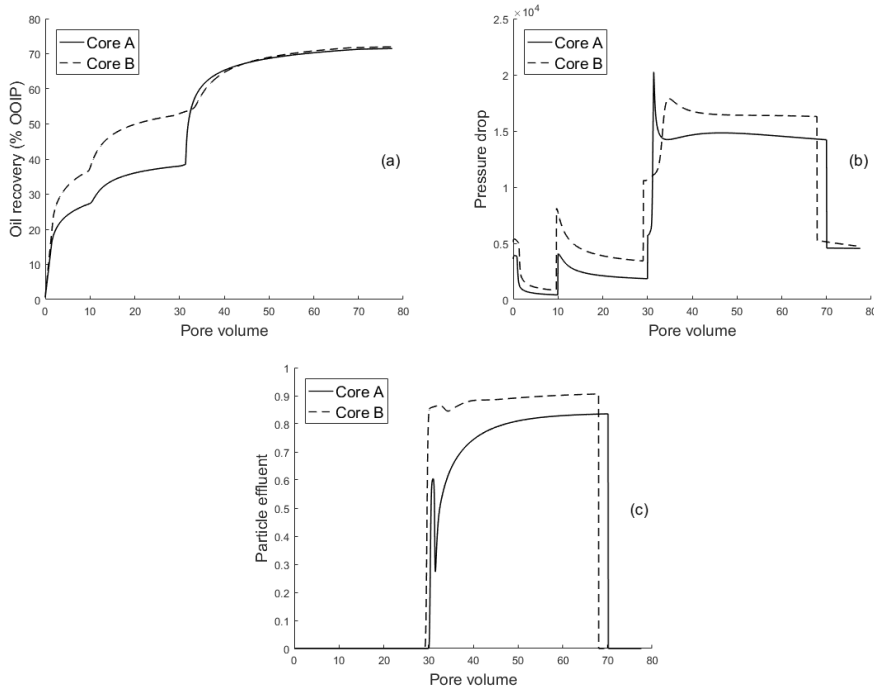

Fig. 7 (a) Oil recovery curves for cores A and B. (b) Pressure drop across the cores A and B. The peaks correspond to oil production and the plateaus to water breakthrough. (c) Particle effluent for cores A and B.

Results for oil production curves for cores A and B are shown in Fig. 7(a). We inject water at a rate of 1.67×10^{-9} m/s for 10 pore volumes, then increase the injection rate up to 1.67×10^{-8} m/s and keep it for 20 pore volumes, when production of oil ceases. Then we start injecting water with polymer particles with a mass concentration of 1 kg/m^3 according to (19). Injection of polymer particles

is sustained for 40 pore volumes, when oil production ceases. The final stage is a postwater flush for 10 pore volumes. These injection periods are longer than the ones reported in (Spildo et al, 2009) because we intended to guarantee that oil production ceased. Since the injection rate is the same for both cores, but core B has a lower permeability, the recovery of oil during waterflood is larger for core B. However, the increase in oil recovery due to polymer particle injection is smaller in core B than in core A. This is a result from the fact that accumulation of particles depends on the heterogeneity of the core as explained previously. Cores with a lower degree of heterogeneity tend to have a slower accumulation of particles, leading to a smaller oil mobilization and therefore resulting in a smaller increase in oil recovery.

During production, the pressure drop along the core increases sharply, followed by a decline after production ceases, when it establishes at a constant value. In Fig. 7(b) we present the pressure drop along the core for cores A and B. The maximum pressure drop occurs at the moment of oil production due to polymer particles injection. The exact value of the maximum pressure drop depends not only on the amount of particles at the effluent, but also on the rock permeability. Since reaction is stronger in core A, more particles are accumulated inside it. This can be seen from Fig. 7(c), where the particle effluent is shown for both cores.

If we denote ΔP_{pw} as the overall pressure drop along the core after the post-water flush and ΔP_{wf_2} as the overall pressure drop along the core after the 2nd waterflood, we can calculate the ratio $IPR = \Delta P_{pw}/\Delta P_{wf_2}$. This quantity accounts for the overall effects of permeability reduction and mobility increase due to clogging and mobilization of initially-trapped oil. In Table 4 we compare experimental and simulation results for the IPR and the lowering in the residual oil saturation. We also present the calculated permeability reduction for each core. As one can see, there is a trend for a lower increase in oil recovery and lower IPR for the more globally homogeneous core (lower value of δ). The more heterogeneous core tend to have more accumulation of particles, which will lead to a higher degree of microscopic diversion of the flow, thus mobilizing more initially-trapped oil. This experimentally-observed trend can be captured by considering a reaction rate depending on the heterogeneity, as was done in the present work.

Table 4 Comparison between experimental and numerical results.

	Core A	Core B	Core C
IPR (Spildo et al, 2009)	2.60	1.40	1.00
IPR (numerical)	2.50	1.40	1.00
% reduction in s_{or} (Spildo et al, 2009)	61.0	42.0	41.0
% reduction in s_{or} (numerical)	54.0	41.0	37.0
% permeability reduction	66.0	42.0	20.0

Note that the reduction in residual oil saturation for cores B and C are similar, although their IPR are significantly different. An experimental value of $IPR = 1$ for core C indicates that the final permeability reduction is very low. This suggests that after oil mobilization takes place, almost total unclogging of the pores occurred. In our model we adjusted the value of the unclogging constant k_l for each core in order to match experimental data. By performing a proper analysis of the problem at the pore scale, one should be able to predict the qualitative

dependence of the reaction rate constants k_r and k_l. Therefore, k_r and k_l will be parameters that depend on the mechanical-physical interactions between the oil-water flow, particle transport and rock geometry at the pore scale.

4 Conclusions

We developed a simple model for the transport of polymer particles in an oil-water flow in a porous medium, which takes into account the clogging/unclogging of pore throats. We show that recent experimental results (Spildo et al, 2009, 2010) can be explained by considering a dynamic alteration of the permeability and a macroscopic degree of the microscopic core heterogeneity. Nevertheless, a detailed derivation of the reaction rates at the pore-scale must be conducted in order to better clarify the complicated coupled physics in this problem.

The transport of polymer particles in a oil-water flow in porous media is a complex problem. In particular, we point to the difficulty in capturing all physical meaningful effects with a heuristic model, without resorting to large-scale experimental fitting. In the limit of severe permeability decrease, i.e., if $K \to 0$, injectivity of water becomes an issue to be addressed. Moreover, in this case the problem will be degenerated, such that the Newton solver embedded in MRST might not have an efficient convergence. In this case, different linearization schemes must be implemented in order to efficiently numerically solve the problem (Radu et al, 2015; List and Radu, 2016). In order to compare with experimental results, we considered essentially a one-dimensional domain. For reservoirs, the large heterogeneities existent may favour formation of fingers by channelling, which compromise oil recovery. Therefore, a stability analysis would be relevant for reservoir applications (Musuuza et al, 2009, 2011). A future work will also consider a more detailed derivation of the clogging/unclogging model.
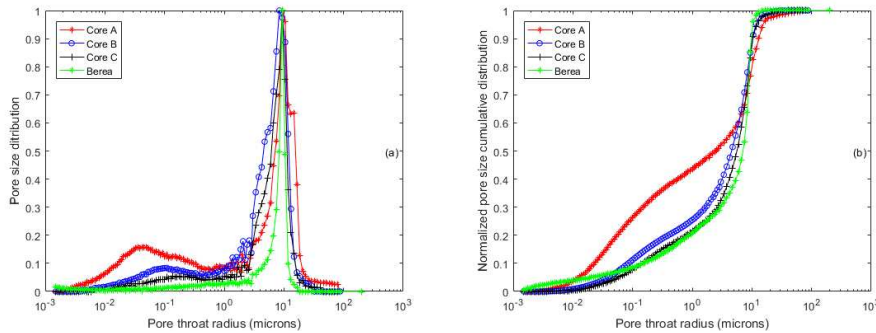
A Heterogeneity factor

Fig. 8 (a) Normalized pore size distribution and (b) normalized cumulative distribution function.

As mentioned previously, a key aspect for the accumulation of particles is the heterogeneity of the core. In Fig. 8(a) we show the normalized pore size distributions and in (b) their respective normalized cumulative distribution functions, for cores A, B and C. We also plot the distribution functions for the Berea core, which is the homogeneous core utilized for comparison. Experiments with polymer particle injection have shown negligible increase in oil recovery for Berea cores (Skauge et al, 2010). Since Berea is a fairly homogeneous core, this supports our claim that heterogeneity plays a significant role in microscopic diversion. Therefore, we chose Berea as a representative homogeneous core for the calculation of the heterogeneity factor δ.
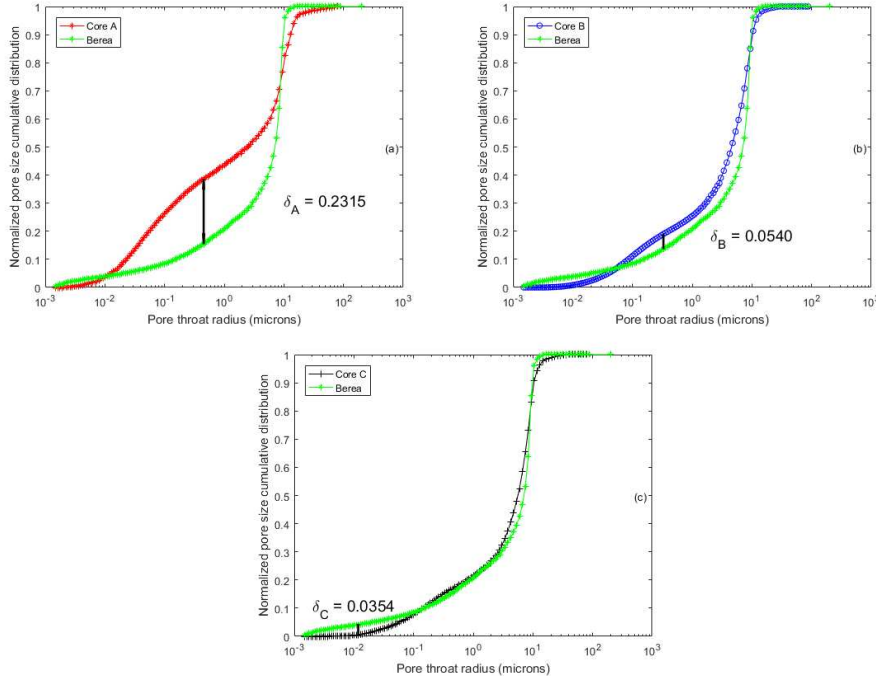

Fig. 9 Heterogeneity factor for cores (a) A, (b) B and (c) C.

In Figs. 9(a) to (c) we present the comparison between cores A to C and the Berea, with their respective values for δ. In essence, δ is a measurement of how far from a homogeneous core (Berea) the given sample is. Larger values of δ gives a high heterogeneity, indicating that the core is more suitable for oil recovery enhancement through polymer particle injection. For convention, pores with radius $r < 1 \ micron$ are considered in the microscopic region, whereas pores with radius $> 1 \ micron$ are at the macroscopic region. We consider the maximum separation between distributions δ in the microscopic region. In other words, we neglect the variations in pore sizes in the macroscopic region ($r > 1 \ micron$). This is justified by the fact that particle-carrying water flow only clogs a pore when the large-to-narrow pore throat ratio is large. In other words, a flow change from two pores with different throat radius does not permit clogging if both pores are in the macroscopic region.

In essence, the heterogeneity factor compares distributions at the microscale. Nevertheless, the parameter δ is dependent on the base distribution used for comparison (Berea, in the present case). If instead of Berea we considered another distribution with a very different pore throat radius range as a base, the different scales for the compared cores would render a wrong calculation for the parameter δ. In fact, a more precise definition and derivation of δ would have to be independent on considering a base core. This will be done in a future work.

References

Abdulbaki M, Huh C, Sepehrnoori K, Delshad M, Varavei A (2014) A critical review on use of polymer microgels for conformance control purposes. J Petroleum Sci Eng 122:741–753

Adler P, Jacquin C, Quiblier J (1990) Flow in simulated porous media. Int J Multiphase Flow 16:691–712

de Anna P, Quaife B, Biros G, Juanes R (2017) Prediction of the low-velocity distribution from the pore structure in simple porous media. Physical Review Fluids 2:124103

Bao K, Lie KA, Myner O, Liu M (2017) Fully implicit simulation of polymer flooding with MRST. Computational Geosciences 21:1219–1244

Bennacer L, Ahfir ND, Alem A, Wang H (2017) Coupled effects of ionic strength, particle size, and flow velocity on transport and deposition of suspended particles in saturated porous media. Transport in Porous Media 118:251–269

Bjørsvik M, Høiland H, Skauge A (2008) Formation of colloidal dispersion gels from aqueous polyacrylamide solutions. Colloids Surf A 317:504–511

Bolandtaba S, Skauge A (2011) Network modeling of eor processes: a combined invasion percolation and dynamic model for mobilization of trapped oil. Transport in Porous Media 89:357–382

Bolandtaba S, Skauge A, Mackay E (2009) Pore scale modelling of linked polymer solution (LPS) - a new EOR process. Paper presented at the 15th European Symposium on Improved Recovery DOI 10.3997/2214-4609.201404822

Borazjani S, Behr A, Genolet L, Van Der Net A, Bedrikovetsky P (2017) Effects of fines migration on low-salinity waterflooding: analytical modelling. Transport in Porous Media 116:213–249

Bringedal C, Kumar K (2017) Effective behavior near clogging in upscaled equations for non-isothermal reactive porous media flow. Transport in Porous Media 120:553–577

Bringedal C, Berre I, Pop I, Radu F (2016) Upscaling of non-isothermal reactive porous media flow with changing porosity. Transport in Porous Media 114:371–393

Brooks R, Corey A (1964) Hydraulic properties of porous media. Colorado State University

Chang H, Xui X, Xiao L, Guo Z, Yao Y, Xiao Y, Chen G, Song K, Mack J (2006) Successful field pilot of in-depth colloidal dispersion gel (CDG) technology in daqing oil field. SPE Reservoir Eval Eng 89460

Civan F (2016) Modified formulations of particle deposition and removal kinetics in saturated porous media. Transport in Porous Media 111:381–410

van Duijn C, Cao X, Pop I (2016) Two-phase flow in porous media: dynamic capillarity and heterogeneous media. Transport in Porous Media 114:283–308

El-Amin M, Sun S, Salama A (2013) Enhanced oil recovery by nanoparticles injection: modeling and simulation. SPE Journal 164333

Gruesbeck C, Collins R (1982) Entrainment and deposition of fine particles in porous media. Soc Petroleum Engineering J pp 847–856

Hussain F, Zeinijahromi A, Bedrikovetsky P, Badalyan A, Carageorgos T, Cinar Y (2013) An experimental study of improved oil recovery through fines-assisted waterflooding. J Petroleum Sci Engineering 109:187–197

Jacquin C (1964) Corrélation entre la perméabilité et les caratéristiques géométriques du grés de fontainebleau. Revue Inst Fr Pétrole 19:921–937

Lake L, Schmidt R, Venuto P (1992) A niche for enhanced oil recovery in the 1990s. Oilfield Reviews pp 55–61

Landa-Marbán D, Radu F, Nordbotten J (2017) Modeling and simulation of microbial enhanced oil recovery recovery including interfacial area. Transport in Porous Media 120:395–413

Li Y, Abriola L, Phelan T, Ramsburg C, Pennell K (2007) Experimental and numerical validation of the total trapping number for prediction of DNAPL mobilization. Environ Sci Technol 41:8135–8141

Lie KA (2016) And introduction to reservoir simulation using MATLAB: User guide for the Matlab Reservoir Simulation Toolbox (MRST). SINTEF ICT

List F, Radu F (2016) A study on iterative methods for solving richard's equation. Computational Geosciences 20:341–353

Mack J, Smith J (1994) In-depth colloidal dispersion gels improve oil recovery efficiency. SPE 27780

Muntean A, Nikolopoulos C (2017) Colloidal transport in locally periodic evolving porous media - an upscaling exercise. arXiv 1712.05598

Musuuza J, Attinger S, Radu F (2009) An extended stability criterion for density-driven flows in homogeneous porous media. Advances in Water Resources 23:796–808

Musuuza J, Radu F, Attinger S (2011) The stability of density-driven flows in saturated heterogeneous porous media. Advances in Water Resources 34:1464–1482

Nasralla R, Nasr-El-Din H (2014) Double-layer expansion: is it a primary mechanism of improved oil recovery by low-salinity waterflooding? SPE Journal 154334

Pope G (1980) The application of fractional flow theory to enhanced oil recovery. SPE Journal

Radu F, Nordbotten J, Pop I, Kumar K (2015) A robust linearization scheme for finite volume based discretizations for simulation of two-phase flow in porous media. J Computational Applied Math 289:134–141

Ray N, van Noorden T, Frank F, Knabner P (2012) Multiscale modeling of colloid and fluid dynamics in porous media including an evolving microstructure. Transport in Porous Media 95:669–696

Sheng J (2011) Modern Chemical Enhanced Oil Recovery: Theory and Practice. Elsevier

Shi J, Varavei A, Huh C, Delshad M, Sepehrnoori K, Li X (2011) Viscosity model of preformed microgels for conformance and mobility control. Energy and Fuels 25:5033–5037

Skauge T, Hetland S, Spildo K, Skauge A (2010) Nano-sized particles for EOR. SPE Journal 129933

Spildo K, Skauge A, Aarra M, Tweheyo M (2009) A new polymer application for North Sea reservoirs. SPE Journal 113460

Spildo K, Skauge A, Skauge A (2010) Propagation of colloidal dispersion gels (CDG) in laboratory corefloods. SPE Journal 129927

Stephens M (1974) EDF statistics for goodness of fit and some comparisons. J American Statistical Association 69:730–737

You Q, Dai C, Tang Y, Guan P, Zhao G, Zhao F (2013) Study on performance evaluation of dispersed particle gel for improved oil recovery. J Energy Resources Tech 135